

# A numerical study on the existence of stable motions near the triangular points of the real Earth-Moon system

## A dynamical systems approach to the existence of Trojan motions

À. Jorba

Universitat de Barcelona, Departament de Matemàtica Aplicada i Anàlisi, Gran Via 585, 08007 Barcelona, Spain (angel@maia.ub.es)

Received 21 March 2000 / Accepted 18 September 2000

**Abstract.** In this paper we consider the existence of stable motions for a particle near the triangular points of the Earth-Moon system. To this end, we first use a simplified model (the so-called Bicircular Problem, BCP) that includes the main effects coming from the Earth, Moon and Sun. The neighbourhood of the triangular points in the BCP model is unstable, as happens in the real system. However, here we show that, in the BCP, there exist sets of initial conditions giving rise to solutions that remain close to the Lagrangian points for a very long time. These solutions are found at some distance from the triangular points.

Finally, we numerically show that some of these solutions seem to subsist in the real system (by real system we refer to the model defined by the well-known JPL ephemeris), in the sense that the corresponding trajectories remain close to the equilateral points for at least 1 000 years. These orbits move up and down with respect to the Earth-Moon plane, crossing this plane near the triangular points. Hence, the search for Trojan asteroids in the Earth-Moon system should be focused on these regions and, more concretely, in the zone where the trajectories reach their maximum elongation with respect to the Earth-Moon plane.

**Key words:** celestial mechanics, stellar dynamics

### 1. Introduction

Let us start by assuming that the Earth and Moon are point masses that revolve in circular orbits around their common centre of mass, and consider a particle with infinitesimal mass under the gravitational attraction of the Earth and Moon (in this context, the Earth and Moon are sometimes called primaries). The study of the dynamics of this third particle is the so-called RTBP. It is usual to take a system of reference with the origin at the centre of mass, and with rotating axes such that the primaries are fixed on the  $x$  axis, the  $y$  axis is contained in the plane of motion of the primaries and orthogonal to the  $x$  axis, and the  $z$  axis is orthogonal to the  $(x, y)$  plane. This system of reference is called synodical. The unit of distance is the distance between primaries, the unit of mass is the total mass of the primaries, and

the unit of time is such that the gravitational constant is one. In these units, the period of the primaries around their common centre of mass is equal to  $2\pi$ . In this system of reference, the Earth and Moon have coordinates  $(\mu, 0, 0)$  and  $(\mu - 1, 0, 0)$ , respectively. It turns out that the equations of motion of the infinitesimal particle can be written in Hamiltonian form, with Hamiltonian function given by

$$H_{\text{RTBP}} = \frac{1}{2}(p_x^2 + p_y^2 + p_z^2) + yp_x - xp_y - \frac{1-\mu}{r_{\text{PE}}} - \frac{\mu}{r_{\text{PM}}},$$

where  $r_{\text{PE}}^2 = (x - \mu)^2 + y^2 + z^2$  is the distance of the particle to the Earth, and  $r_{\text{PM}}^2 = (x - \mu + 1)^2 + y^2 + z^2$  the distance of the particle to the Moon. It is well known (Szebehely 1967; Meyer & Hall 1992) that, in synodical coordinates, the RTBP has five equilibrium points, three of them lie on the  $x$  axis (they are also called Euler points, collinear points or simply  $L_1$ ,  $L_2$  and  $L_3$ ) and two of them are the third vertex of an equilateral triangle that has the primaries as the other vertices (they are also called Lagrangian points, triangular points or  $L_4$  and  $L_5$ ).

We start focusing on the dynamics around the equilateral point  $L_5$  of the RTBP (the same results will hold for  $L_4$  due to the symmetries of this model). For the value of the mass corresponding to the Earth-Moon case,  $L_5$  is an elliptic equilibrium point. Under very general conditions, standard results from KAM theory (Arnold et al. 1988) predict that, around an elliptic equilibrium point of a Hamiltonian system, there exist many quasi-periodic solutions. In suitable coordinates (the so-called action-angle variables), these solutions correspond to linear motions taking place on invariant tori, whose dimension coincides with the number of basic frequencies of the quasi-periodic motion. For this reason, in this context it is usual to refer to quasi-periodic solutions as invariant tori. Due to the constraints imposed by the Hamiltonian structure, the dimension of these tori (i.e., the number of basic frequencies of the quasi-periodic motions) cannot be greater than half the dimension of the phase space. In this sense, we will distinguish between the maximal dimensional tori (tori whose dimension equals half the dimension of the phase space) and lower dimensional tori. It is well known that the set filled by the maximal dimensional tori has positive measure and empty interior. Obviously, initial conditions inside

this set give rise to trajectories that are always close to the equilibrium point. So, to study the instability of an elliptic point we should look at the dynamics on the complementary of the tori set. The (possible) diffusion inside this set is usually called Arnold diffusion (Arnold 1964). The main results in this direction are only upper bounds on the diffusion speed (Giorgilli et al. 1989; Simó 1989; Celletti & Giorgilli 1991; Jorba & Villanueva 1997a; Giorgilli & Skokos 1997; Benettin et al. 1998; Niederman 1998). One of the main conclusions of these works is that, under general conditions, the time needed to escape from a neighbourhood of the equilibrium point is (at least) exponentially large with respect to the distance from the initial condition to the equilibrium point. Hence, the application of these results to the RTBP corresponding to the Earth-Moon case results in very large stability times. This kind of stability is usually called effective stability.

On the other hand, we can consider the motion of a small particle in the real Solar system, in a neighbourhood of the triangular points of the Earth and Moon. Here, we will use as “real Solar system” the model defined by the JPL ephemeris (<http://ssd.jpl.nasa.gov/horizons.html>). This is a numerically defined vector field, that can be numerically integrated for the time span for which the positions of the main bodies are known. Note that, for the real system, the triangular points are no longer equilibrium points since the hypotheses used to derive the RTBP are not satisfied. It is known that arbitrary trajectories starting near the (geometrically defined) triangular points move away after a short time (Schutz & Tapley 1970; Díez et al. 1991) and hence, the RTBP is not a good model to study this problem because it displays a qualitative behaviour that is quite different.

For this reason, we will start using the so called Bicircular Problem (from now on, BCP). This model can be seen as a time dependent periodic perturbation of the RTBP, that includes the main effect coming from the Sun. We believe that this model was first introduced by Cronin et al. (1964), and it has some of the main features of the real model (for instance, the neighbourhood of the equilateral points is unstable). Our purpose is to use the BCP as a first model to describe some properties of the real system. In particular, it is known that the BCP has several families of quasi-periodic solutions near the equilateral points (Simó et al. 1995; Jorba 1998; Castellà & Jorba 2000). It turns out that some of these tori are hyperbolic, while some others are elliptic (Jorba 1998, 2000), and that these elliptic tori are found at some distance from the equilateral points. It is known that lower-dimensional normally elliptic tori give rise, under general conditions, to regions of effective stability around them (Jorba & Villanueva 1997a,b). Here, we will estimate the size and shape of these regions by means of numerical simulations, to show that they are relevant for this problem.

The last step will be to show, by means of numerical simulations, that some of the stability regions found in the BCP model subsist in the real system, at least for time spans of 1 000 years. As will be discussed later (in Sect. 5), these regions are a suitable place to look for Trojan asteroids in the Earth-Moon system.

This kind of stability was previously observed (Gómez et al. 1993; Simó et al. 1995), but with smaller regions and much shorter time intervals (around 60 years). The main improvements in this work come from the computation of the vertical families of quasi-periodic solutions for the BCP and the use of initial conditions around them. It seems that these families of tori are the skeleton that supports these stability regions. A preliminary version of these results was presented in a conference paper (Jorba 1998).

## 2. The bicircular model

The bicircular model is a Restricted Four-Body Problem that can be seen as a modification of the RTBP in order to take into account (in an approximate way) the effect of the Sun. We refer to Cronin et al. (1964) for a detailed derivation of the equations of motion.

To define this model, we impose that: a) the Earth and Moon revolve in circular orbits around their centre of mass (as in the RTBP); and b) the Earth-Moon barycentre and the Sun also move in circular orbits around the Earth-Moon-Sun centre of mass, that is fixed at the origin. Of course, these two circular motions satisfy Kepler’s laws. Then, it is not difficult to derive the equations of motion of a fourth (infinitesimal) particle moving under the attraction of these three bodies. The study of the motion of this fourth particle is the so-called BCP. Note that, in this model, the motion of the Earth, Moon and Sun is not coherent, since it does not follow a true solution of the Three-Body Problem.

To write the equations of motion of the BCP, we use the same reference frame as in the RTBP: the origin is taken at the centre of mass of Earth and Moon, the  $x$  axis is on the Earth-Moon line, the  $y$  axis is contained in the plane of motion of Earth and Moon, and the  $z$  axis is orthogonal to the  $(x, y)$  plane (see Fig. 1). In this system of reference, the Sun is turning (clockwise) around the origin in a periodic way. As in the RTBP, we use normalized units such that the Earth-Moon distance is 1, the total mass of the Earth-Moon system is 1, and the period of Earth and Moon around their barycentre is  $2\pi$ . In these units, we denote by  $a_S$  the distance from the Earth-Moon barycenter to the Sun,  $m_S$  is the mass of the Sun, and the frequency of the motion of the Sun around the origin is denoted by  $\omega_S$ . In these coordinates,  $\omega_S$  is the sidereal frequency of the Sun minus 1.

Let  $(x, y, z)$  be the coordinates of the infinitesimal particle. Then, defining the corresponding momenta as  $p_x = \dot{x} - y$ ,  $p_y = \dot{y} + x$  and  $p_z = \dot{z}$ , the motion of the fourth particle can be described by a Hamiltonian system that depends on time in a periodic way:

$$H_{\text{BCP}} = \frac{1}{2} (p_x^2 + p_y^2 + p_z^2) + yp_x - xp_y - \frac{1-\mu}{r_{\text{PE}}} - \frac{\mu}{r_{\text{PM}}} - \frac{m_S}{r_{\text{PS}}} - \frac{m_S}{a_S^2} (y \sin \theta - x \cos \theta),$$

where  $r_{\text{PE}}^2 = (x-\mu)^2 + y^2 + z^2$ ,  $r_{\text{PM}}^2 = (x-\mu+1)^2 + y^2 + z^2$ ,  $r_{\text{PS}}^2 = (x-x_S)^2 + (y-y_S)^2 + z^2$ ,  $x_S = a_S \cos \theta$ ,  $y_S =$

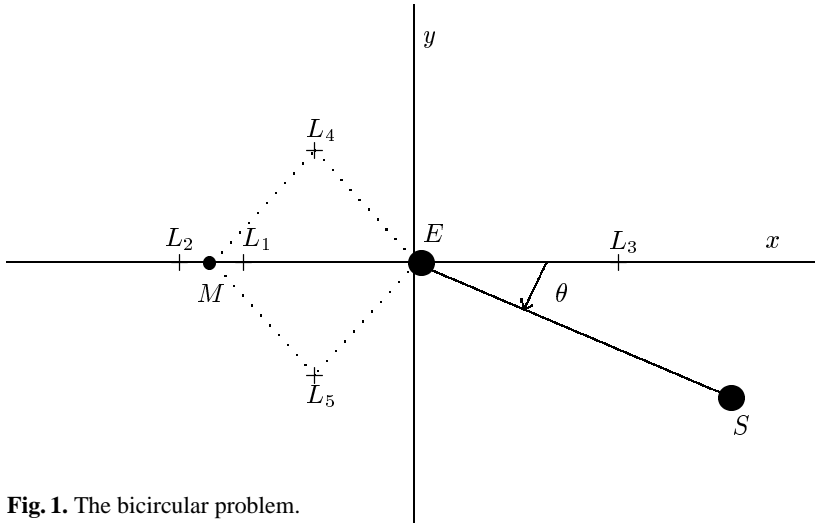
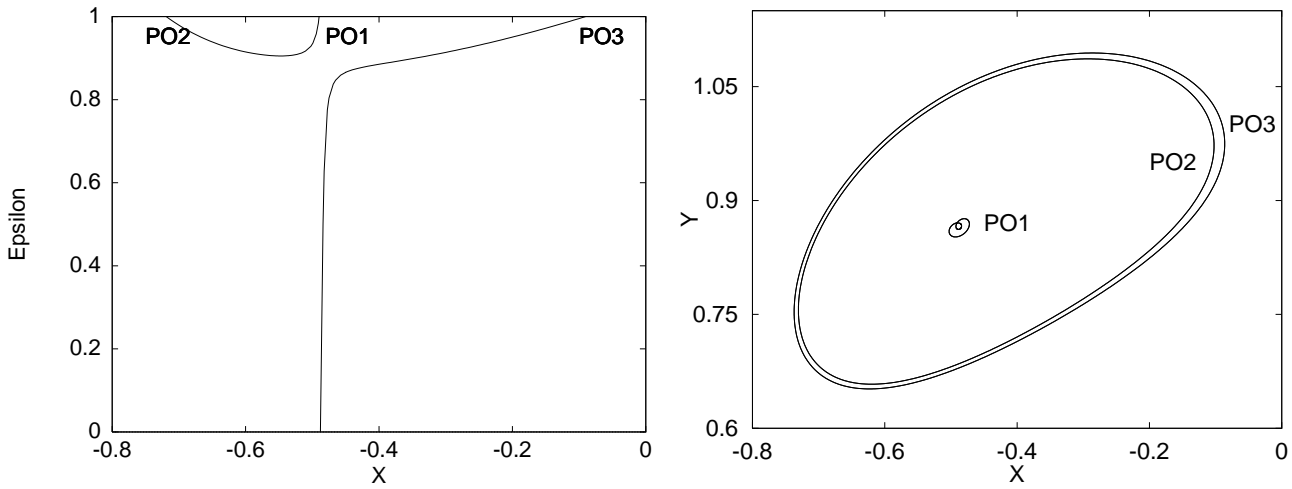


Fig. 1. The bicircular problem.


 Fig. 2. Left: Continuation of the periodic orbit that replaces  $L_5$  in the BCP. Right: The three periodic orbits that appear in the left plot for  $\varepsilon = 1$ .

$-a_S \sin \theta$ , and  $\theta = \omega_S t$ . We stress that we can look at the BCP as a periodic time dependent perturbation of the RTBP:

$$H_{\text{BCP}}^\varepsilon = H_{\text{RTBP}} + \varepsilon \hat{H}_{\text{BCP}},$$

where

$$\hat{H}_{\text{BCP}} = -m_S \left( \frac{1}{r_{\text{PS}}} + \frac{y \sin \theta - x \cos \theta}{a_S^2} \right),$$

and it is clear that  $H_{\text{BCP}}^{\varepsilon=0} = H_{\text{RTBP}}$ , and that  $H_{\text{BCP}}^{\varepsilon=1} = H_{\text{BCP}}$ . In Fig. 1 we have marked the Eulerian and Lagrangian points  $L_{1,\dots,5}$  by using their corresponding coordinates in the RTBP. As the vector field of the perturbation  $\varepsilon \hat{H}_{\text{BCP}}$  does not vanish at these points, they are no longer equilibrium solutions.

Now, we focus on the  $L_5$  point (due to the symmetries of the BCP, the same results will be valid for  $L_4$ ; of course, this is not true for the real system). A straightforward application of the Implicit Function Theorem shows that, under a generic non-resonance condition (satisfied in this case) and assuming  $\varepsilon$  small enough,  $L_5$  is replaced by a periodic orbit with the same period as the perturbation. This orbit tends to  $L_5$  when  $\varepsilon$  tends to zero.

To reduce the number of degrees of freedom of the problem, we introduce the Poincaré section  $t = 0 \bmod T_S$ , where  $T_S = 2\pi/\omega_S$  is the period of the perturbation, and let  $P_\varepsilon$  be the corresponding Poincaré map. Note that  $P_\varepsilon$  is an autonomous 6-D (symplectic) map whose fixed points correspond to periodic orbits (of period  $T_S$ ) for the flow, and vice versa.

Now, by means of a continuation process, we compute the fixed points of  $P_\varepsilon$  (for  $\varepsilon$  ranging between 0 and 1) that correspond to the periodic orbit that replaces  $L_5$ . The results are displayed in Fig. 2 (left), where the horizontal axis shows the  $x$  coordinate of the fixed point and the vertical axis refers to the value of  $\varepsilon$ . Note that, for  $\varepsilon = 1$ , there are three fixed points of  $P_\varepsilon$  that are close to  $L_5$ . The  $(x, y)$  projection of the corresponding periodic orbits for the flow are displayed in Fig. 2 (right). By computing the eigenvalues of the differential of  $P_\varepsilon$  at the fixed points, one can see that orbit PO1 is unstable, and that orbits PO2 and PO3 are linearly stable. Moreover, these three periodic orbits have an elliptic mode contained in the  $(z, p_z)$  plane. In what follows, we will refer to this mode as the vertical mode of the corresponding periodic orbit. More details about the BCP can be found in the literature (Gómez et al. 1993; Simó et al. 1995).

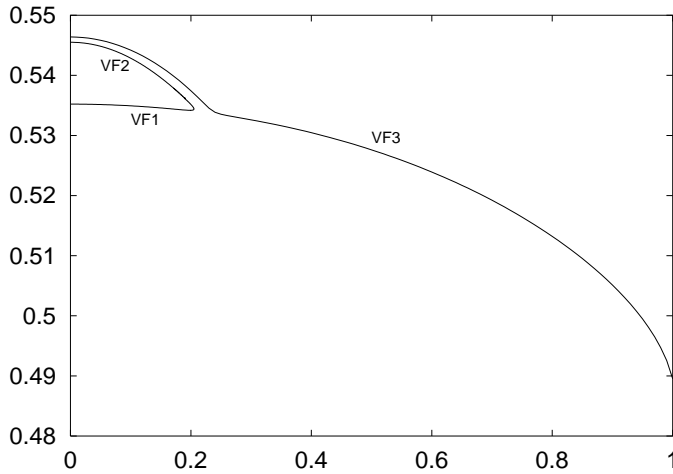


**Fig. 3.** The vertical families of 2-D tori. The graphic corresponds to the map  $P_\varepsilon$ , for  $\varepsilon = 1$ . The horizontal axis is the  $z$  coordinate, and the vertical axis displays the rotation number. See the text for more details.

### 2.1. The vertical families of 2-D tori of the BCP

Let us now consider the vertical mode of one of the periodic orbits. It is known that, under generic conditions (Jorba & Villanueva 1997a,b), there exists a Cantor family of 2-D invariant tori that extend this linear mode into the complete (i.e., nonlinear) system. This is very similar to the well-known Lyapunov centre theorem, but instead of obtaining a (smooth) family of periodic orbits, one obtains a (Cantor) family of quasi-periodic solutions, with two (linearly independent) basic frequencies. In suitable coordinates, each quasi-periodic solution fills densely a two dimensional torus. Hence, for each periodic orbit PO1, PO2 and PO3, there is a Cantor family of 2-D tori (let us call them VF1, VF2 and VF3, respectively) that “grows up” in the vertical direction.

In order to display these families, we use again the map  $P_\varepsilon$  defined before. In this way the 2-D tori become invariant curves of a 6-D symplectic map. As all these curves cross transversally the hyperplane  $z = 0$ , we select, for each curve, the only point on the invariant curve that has  $z = 0$  and  $\dot{z} > 0$ . Thus, each curve is represented by a single point. We have used this representation in Fig. 3. The horizontal axis displays the  $z$  coordinate while the vertical axis contains the rotation number of the invariant curve. Note that families VF1 and VF2 are connected (as suggested by the connection of the periodic orbits PO1 and PO2 in Fig. 2), while VF3 reaches high amplitudes in the  $(z, \dot{z})$  direction. In fact, as the projection of these quasi-periodic motions in the  $(z, \dot{z})$  plane is close to an harmonic oscillator (see also Sect. 3.2), the value of  $\dot{z}$  when  $z = 0$  is a good approximation to the maximum value reached by the  $z$  coordinate. The details about these computations can be found in Jorba (1998) and Castellà & Jorba (2000).

It is also known that, under generic hypotheses of non-resonance, the tori on these families that are close to the basic periodic orbits have the same stability as these periodic orbits. So, for moderate vertical amplitudes, we expect the tori on VF1 to be hyperbolic, and most of the tori on VF2 and VF3 to be

elliptic. Families VF1 and VF2 are connected through a turning point, and this is where the change of stability takes place. Family VF3 can be continued up to very high values of the vertical amplitude and, except for small intervals of instability (produced by some resonances involving internal and normal frequencies), the tori in this family are normally elliptic. For more details on the normal stability of these families see Jorba (1998; 2000).

Recent results show that normally elliptic lower dimensional tori are surrounded by a region of effective stability (Jorba & Villanueva 1997a). This means that the time needed to escape from a neighbourhood of one of those tori increases exponentially with the initial distance to the torus. A possibility for estimating the size of this region and the speed of diffusion is to compute a normal form around the torus and to derive estimates on the remainder, as has already been done for periodic orbits (Jorba & Simó 1994; Jorba & Villanueva 1998). Of course, obtaining “analytical” bounds usually requires the use of rather pessimistic inequalities that lead us to underestimate the region where the diffusion is small enough. Here, to have a realistic estimate of the size and shape of this region, we will simply use a numerical simulation to detect initial conditions for which the corresponding trajectory remains there for a sufficiently large time interval. In what follows, we will use the words “quasi-stable region” to refer to a region such that the time taken to escape from it is bigger than a large prescribed value (this value will be specified later on).

### 2.2. Numerical simulations

As it has been mentioned in Sect. 2.1, the families of 2-D tori VF1, VF2 and VF3 correspond to families of invariant curves for the map  $P_{\varepsilon=1}$ . Moreover, on each family, the invariant curves can be “labeled” by the value of the  $z$  coordinate when  $z = 0$  and  $\dot{z} > 0$ . Let  $C(\dot{z}_0)$  be one of these curves, and let  $a(\dot{z}_0) \in \mathbf{R}^6$  be the point on the curve such that  $z = 0$  and  $\dot{z} = \dot{z}_0 > 0$ . The next step is to select a set of initial conditions around the point  $a(\dot{z}_0)$ . To reduce the amount of computations, we will use a two dimensional grid: the coordinates  $z$ ,  $p_x$ ,  $p_y$  and  $p_z$  are fixed by the corresponding values of  $a(\dot{z}_0)$ , and the values of  $x$  and  $y$  are used to define the mesh. Due to the shape of this regions (this will be clear later on), we will use the following polar-like grid,

$$\begin{cases} x_{ij} = r_i \cos \alpha_j + \mu, & r_i = 1 + ih_r, \\ y_{ij} = r_i \sin \alpha_j, & \alpha_j = 2\pi j h_\alpha, \end{cases}$$

where  $h_r$  and  $h_\alpha$  are used to select the density of the mesh and the (integer) indices  $i$  and  $j$  move on suitable ranges, such that the mesh is (approximately) centered around the  $(x, y)$  coordinates of  $a(\dot{z}_0)$ . Then, we will use each point on the grid as an initial condition for a numerical integration of the vector field of the BCP. To decide whether the trajectory escapes, after each time step of the numerical integrator (see Sect. 4), the program uses a couple of tests. First, it checks the actual distance to the Earth and Moon. If the distance to the primaries were lower than their respective radius, then the initial condition would not be considered as belonging to the

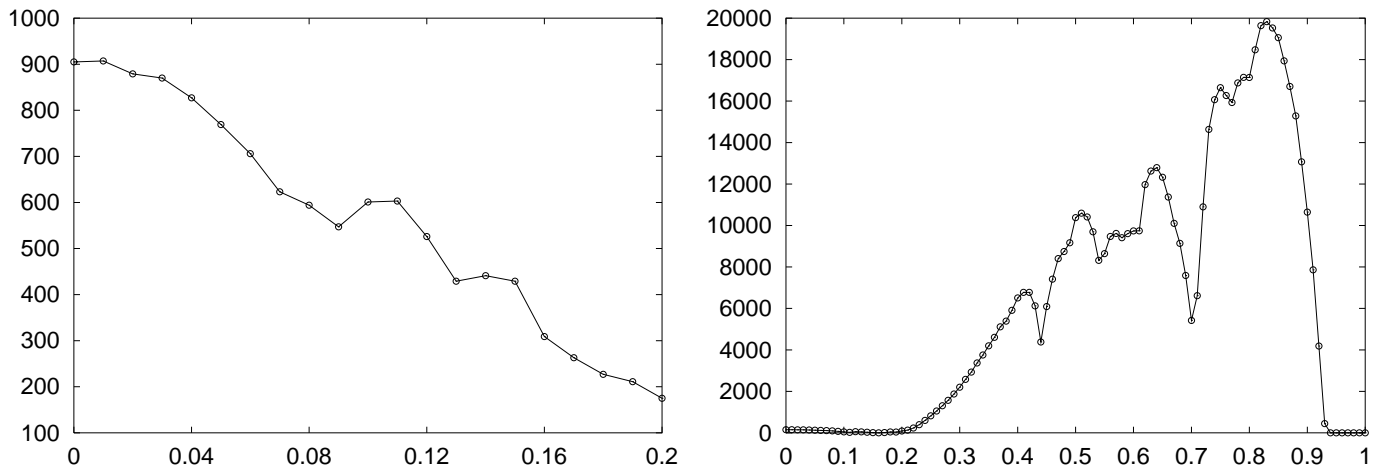


**Fig. 4.** Estimation of the size of the quasi-stable region for the BCP model. The horizontal axis shows the value of  $\hat{z}$  (see the text), and the vertical axis contains the number of points inside the quasi-stable region. Left: Family VF2. Right: Family VF3.

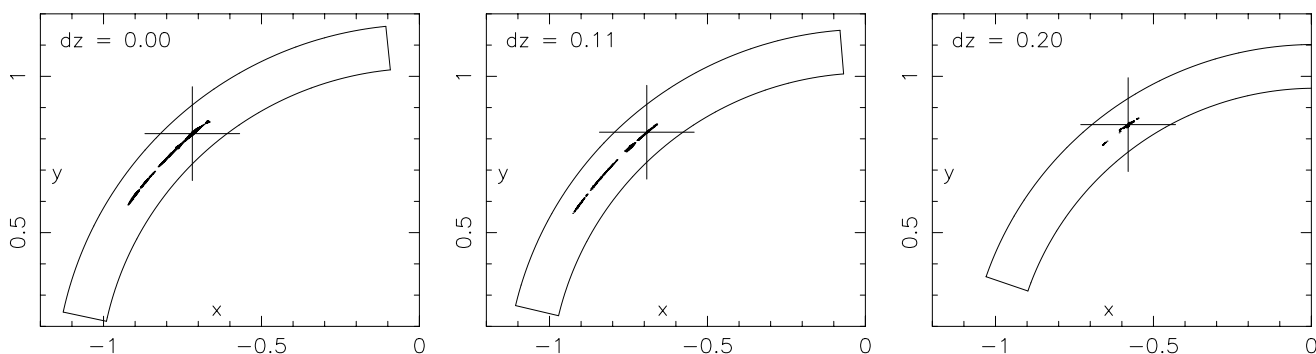


**Fig. 5.** Slices of the quasi-stability regions around the Family VF2 in the BCP. The horizontal and vertical axis are the  $x$  and  $y$  coordinates, respectively. The central quasi-periodic trajectory has been marked with a big “+” sign, and the initial conditions corresponding to non-escaping trajectories are marked with black dots.

quasi-stable region. The second test is to check whether the actual point has crossed the  $y = -0.5$  plane (we recall that we are working around the  $L_5$  point). Numerical experiments show that this last condition is equivalent to escape. This has already been used before (sometimes with different values for the  $y$  section) in several works (McKenzie & Szebehely 1981; Szebehely & Premkumar 1982; Gómez et al. 1993; Simó et al. 1995). In this work, we have used the values  $h_r = 0.001$  and  $h_\alpha = 0.0002$ . The different sizes between these two values is to produce a nearly squared grid. For the numerical integrations, we have used a time interval of 15 000 Moon revolutions (we recall that, in the BCP model, this is equivalent to  $15\,000 \times 2\pi$  units of time).

The results are summarized in Fig. 4 for the VF2 and VF3 families. The horizontal axis displays the same value of  $\hat{z}$  used in the previous section (see also the horizontal axis of Fig. 3). The vertical axis displays the number of non escaping points after 15 000 Moon revolutions. As we have used the same mesh throughout, the number of non escaping points is a good estimate of the size of the stable region. For the Family VF2 the region is not very large, and its size decreases when the value of  $\hat{z}$  increases; this is a natural result since Family VF2 becomes hyperbolic when it meets VF1 (Jorba 1998, 2000). Family VF3

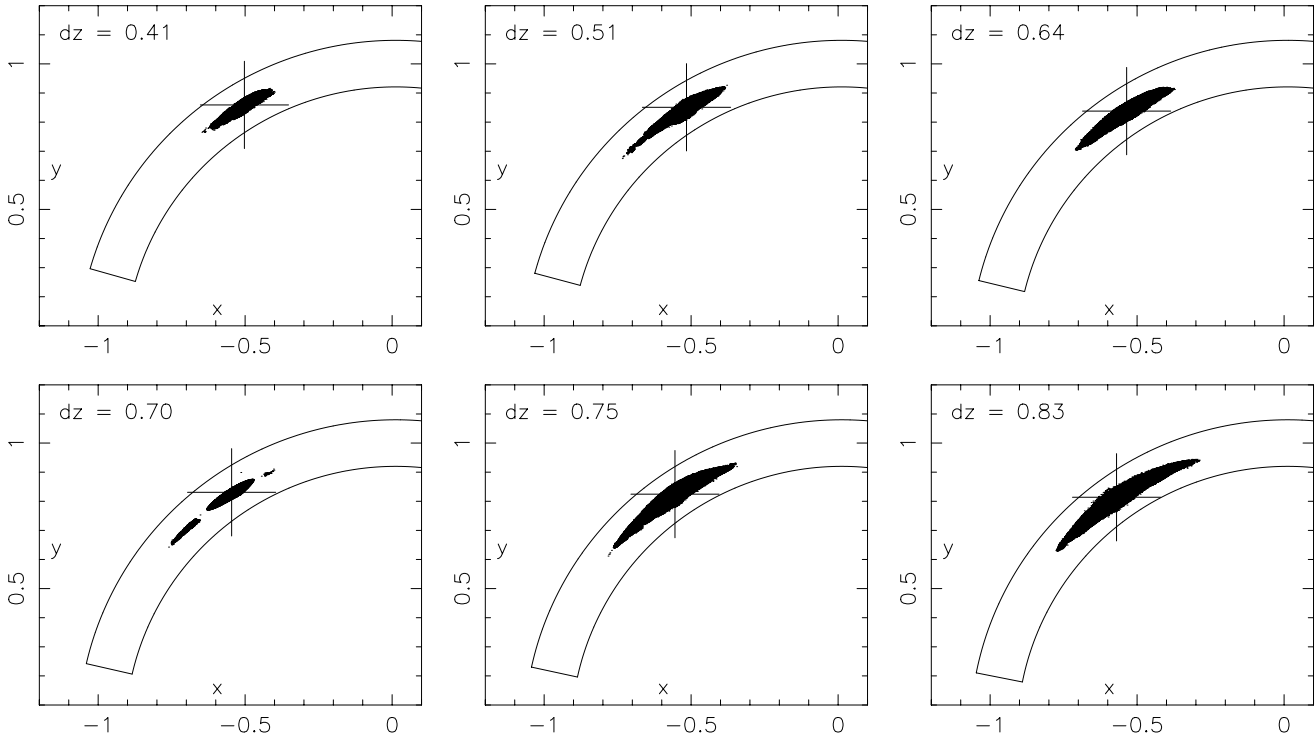
has a bigger stability when  $\hat{z}$  ranges from 0.26 and 0.92 (when  $\hat{z}$  is below 0.20, the size of the region associated to VF3 is in fact smaller than the VF2 one).

Fig. 5 contains a few slices of the stability region around VF2. In each plot we have marked with black dots the initial conditions that do not escape after an integration time of 15 000 Moon revolutions. The large cross in the graphic denotes the intersection of the invariant curve with this slice. The region explored has been drawn with a semi-circular box.

Several slices for Family VF3 are displayed in Fig. 6. These slices correspond to the biggest parts of the region (see Fig. 4). We recall that that the unit of distance in these plots is the Earth-Moon distance, so the size of the displayed regions is quite large in the physical system. As has been mentioned before, it is worth noting that the largest part of the region corresponds to high values of the  $\hat{z}$  coordinate.

### 2.3. Remarks

As has been explained before, the vertical families of quasi-periodic solutions are seen as invariant curves of the map  $P_{\varepsilon=1}$ . To reduce the number of numerical simulations, we have restricted the search of the stable region by selecting a single point



**Fig. 6.** Slices of the quasi-stability regions around the Family VF3 in the BCP. The horizontal and vertical axis are the  $x$  and  $y$  coordinates, respectively. The central quasi-periodic trajectory has been marked with a big “+” sign, and the initial conditions corresponding to non-escaping trajectories are marked with black dots.

on the invariant curve (the one having  $z = 0$  and  $\dot{z} > 0$ ), and taking a 2-D mesh around this point. This mesh is obtained by moving the  $(x, y)$  values of this point and keeping the remaining coordinates constant. Note that this produces a concrete slice of the stable region. The computation of the full region would require a 5-D mesh, obtained by varying 5 coordinates around the initial point ( $\dot{z}$  should be kept fixed to avoid changing the base invariant curve). This process can be applied to every invariant curve on the family (i.e., moving  $\dot{z}$ ), and this will produce an estimate of the full (6-D) region for the map  $P_{\varepsilon=1}$ . The total region for the BCP still requires us to take all the points of the stable region for  $P_{\varepsilon=1}$  as initial conditions, and to integrate them for a period of the time variable  $t$ . This would produce a 7-D region inside the 7-D phase space of the (flow of the) BCP. In other words, the 2-D slice that we have computed in the previous section is the result of taking the full 7-D region for the BCP when  $t = 0$  (a 6-D section), fix  $z = 0$  (5-D section), and fix  $\dot{z}$  and the momenta  $p_x$  and  $p_y$  to suitable values to define the final 2-D slice. The computation of the 7-D quasi-stable region would require a prohibitive amount of computer time and memory. This is the main reason for restricting the simulations to a two-dimensional slice.

### 3. The JPL model

In this section, we will check the quasi-stability results for a very realistic model of Solar system. The model used here is defined by the Jet Propulsion Laboratory (JPL) ephemeris, file

DE406. The JPL ephemeris comprises files containing interpolatory polynomials for the orbital data of each planet, including the Sun, Earth and Moon. These data can be easily used to derive the vector field acting on an infinitesimal particle under the attraction of the main bodies of the Solar system. Of course, this (numerically obtained) vector field is only defined for the time interval for which the ephemeris is provided.

#### 3.1. Numerical simulations

The initial time for the numerical integration is the modified Julian day 20.1978749133 (day 0.0 corresponds to year 2000.0), that coincides with the first full Moon of year 2000.<sup>1</sup> This is to have an initial relative position of the Earth, Moon and Sun similar to the one of the BCP for  $t = 0$ . The simulation stops at year 3000.0. We have also used the same mesh as in the BCP model (see Sect. 2.2). Due to the lack of symmetry between  $L_4$  and  $L_5$  in the real system, we have carried out simulations for both cases. The results obtained are very similar, and are discussed in the following sections.

##### 3.1.1. Stability around the family VF2

In order to compare these results with the ones for the BCP, we have used the same mesh as in Sect. 2.2. Fig. 7 shows the number of initial conditions corresponding to trajectories that do not escape (in the same sense as in Sect. 2.2) for time spans of

<sup>1</sup> In fact, this is the date of the first lunar eclipse of year 2000.

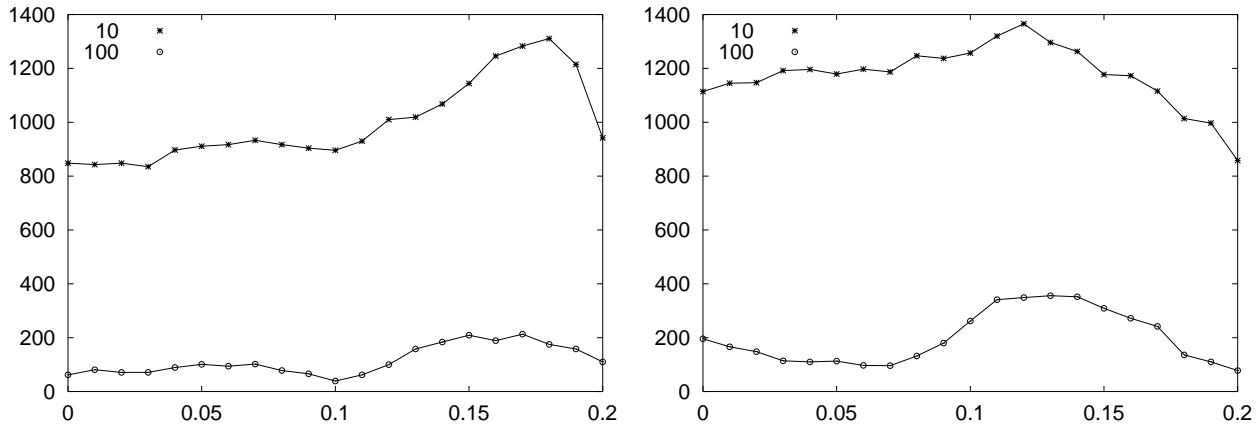


**Fig. 7.** Estimation of the size of the quasi-stable region corresponding to the family VF2 for the JPL model. The upper curve (marked with \*) is for an integration time of 10 years. The lower curve (marked with o) corresponds to an integration time of 100 years. Left:  $L_4$  case. Right:  $L_5$  case. See the text for more details.

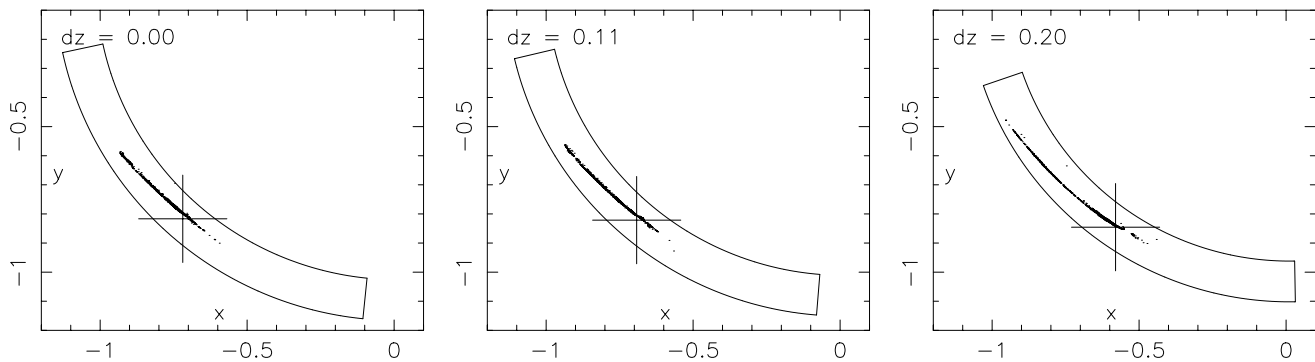


**Fig. 8.** Quasi-stability regions (for a time interval of 10 years) near  $L_4$  around the Family VF2 in the JPL model.

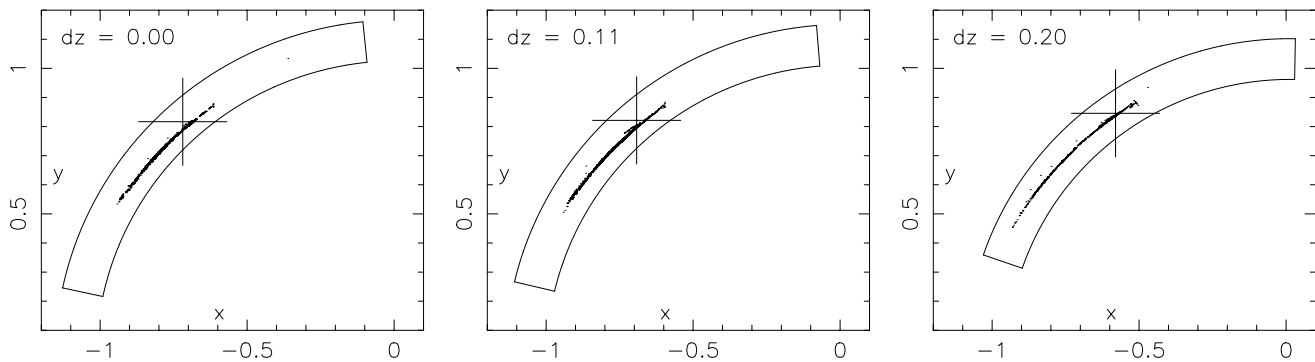


**Fig. 9.** Quasi-stability regions (for a time interval of 10 years) near  $L_5$  around the Family VF2 in the JPL model.

10 years (upper curve) and 100 years (lower curve). We do not include the results for 1 000 years because only a few trajectories subsist: in the  $L_4$  case, the number of these points is never greater than 8, while for the  $L_5$  case this number is slightly bigger (the more stable section corresponds to the case  $\dot{z} = 0.13$ , that contains 85 surviving points). Taking into consideration these results and the behaviour around the family VF2,  $L_5$  seems slightly more stable than  $L_4$ . Moreover, if the integration time were long enough, we believe that all these trajectories would finally escape.

Note the size of the quasi-stable region for a time interval of 10 years (see Figs. 8 and 9). Although a stability time of 10 years is totally irrelevant for astronomical purposes, it could be interesting for astronautical applications, since there would be no need for any kind of control to keep a spacecraft there. The strategy to transfer a spacecraft from a parking orbit to these regions is not considered here. Roughly speaking, a transfer by means of a double lunar swing-by from the standard Ariane Geostationary Transfer Orbit to the vicinity of the triangular points can be completed in about 2 months using a little bit less

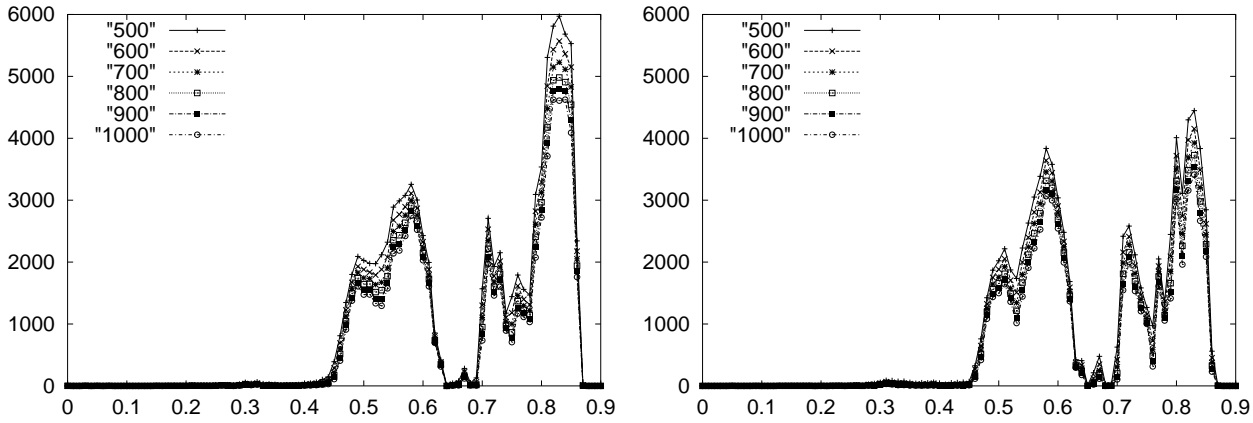


**Fig. 10.** Estimation of the size of the quasi-stable region corresponding to the family VF3 for the JPL model. The plot contains different curves corresponding to several quasi-stability times, ranging from 500 (upper curve) to 1000 years (lower curve). Left:  $L_4$  case. Right:  $L_5$  case. See the text for more details.

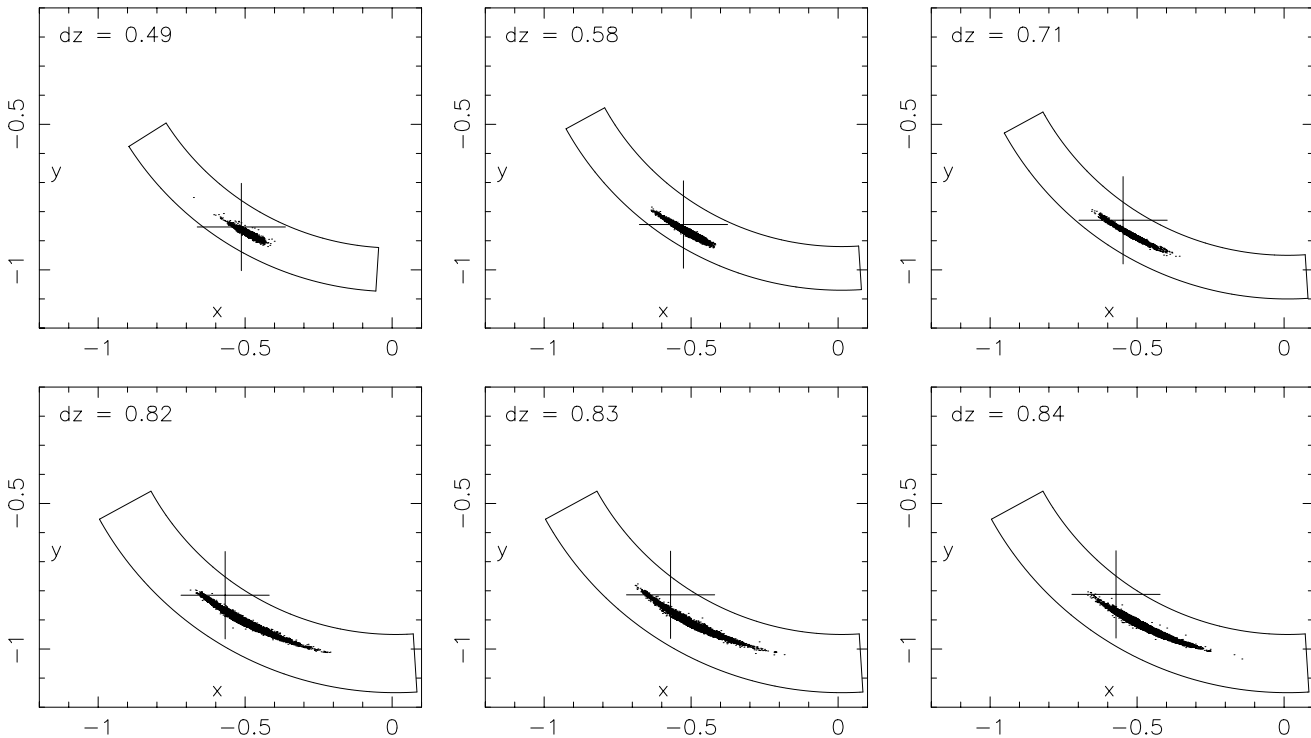


**Fig. 11.** Quasi-stability regions (for a time interval of 1000 years) near  $L_4$  around the Family VF3 in the JPL model.

than 900 m/s of  $\Delta v$  (Companys et al. 1996). For a dynamical systems approach to similar transfers, see also Gómez et al. (1993).

### 3.1.2. Stability around the family VF3

This family seems to be responsible for the largest quasi-stability regions that we have found near to the Lagrangian points. Fig. 10 shows the number of initial conditions corresponding to non escaping trajectories (this is the same plot as in Fig. 4 but for the JPL model). As we have used the same parameters to define the mesh of initial conditions, the “units” in these plots –the vertical axis– are also the same as in the BCP.

So, although the stability region for the JPL model is smaller than that of the BCP, it is remarkable that there exists a quite large stability region for a time span of 1000 years. In order to compare with the simulations for the BCP model, note that 1000 years is more than 13 000 revolutions of the Moon around the Earth.

Figs. 11 and 12 show the  $(x, y)$  coordinates of a few slices of the quasi-stability region for a time interval of 1000 years near the triangular points  $L_4$  and  $L_5$ , respectively. The selected slices correspond to places in which the region is quite large, according to Fig. 10. We recall that the unit of distance is the Earth-Moon distance for the modified Julian day 20.1978749133, that is, 384 467 km.

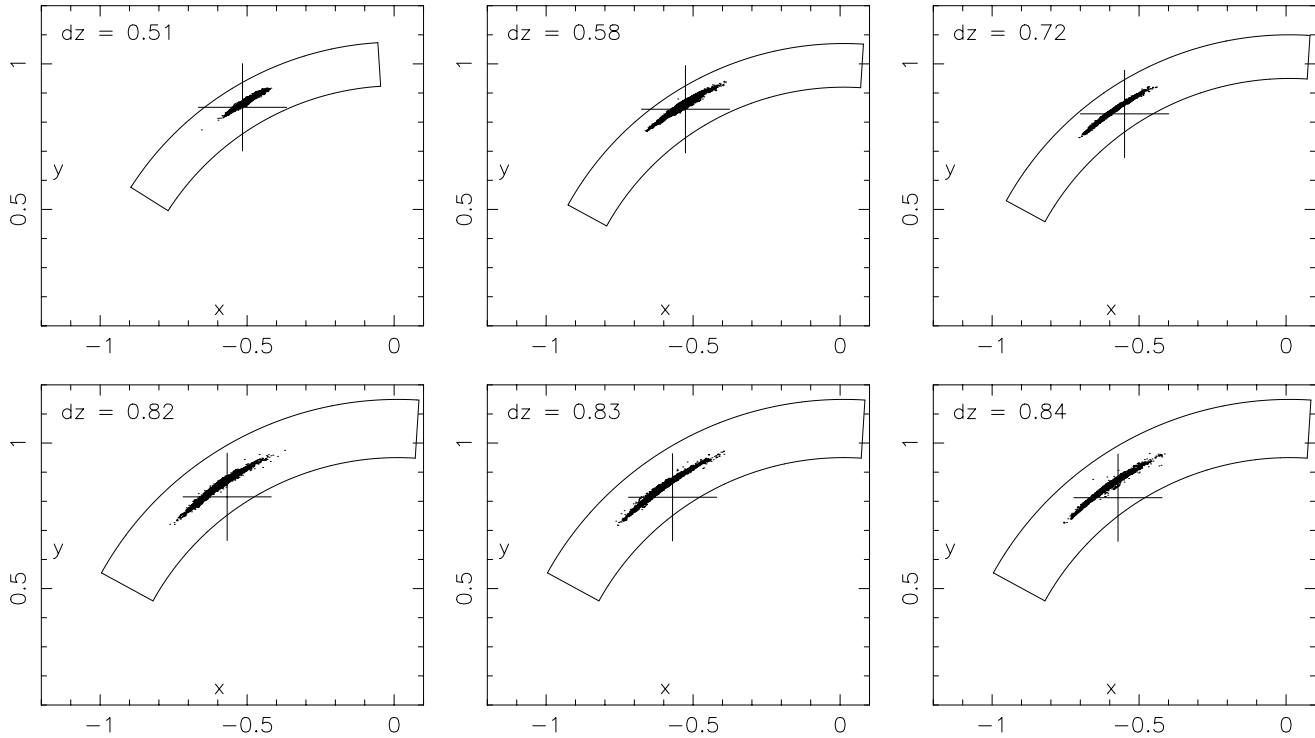


**Fig. 12.** Quasi-stability regions (for a time interval of 1 000 years) near  $L_5$  around the Family VF3 in the JPL model.

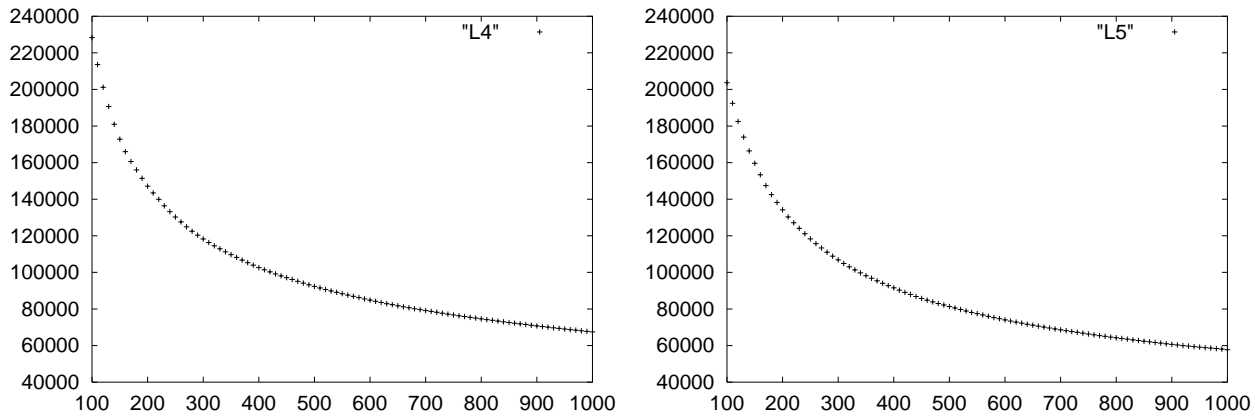


**Fig. 13.** Total number of non escaping initial conditions (vertical axis) against integration time (horizontal axis) around the family VF3. Left:  $L_4$  case. Right:  $L_5$  case.

From these plots, it seems that the BCP model contains several features of the JPL system. This is especially true for the location of the quasi-stability regions, as has been shown by these calculations. However, the comparison between Figs. 4 (right) and 10 also shows that not all the features of JPL are contained in BCP. We believe that these differences are mainly due to resonances in JPL that are not present in BCP, due to the simplicity of the latter. The development and study of improved models is the subject of work in progress.

Obviously, the size of these regions could depend on the length of the integration time. To try to show this dependence, we have carried out the following calculation. To fix the discussion, let us focus on the  $L_4$  point, and let  $C_j$  be the orbit on the family

VF3 for which  $\dot{z} = j/100$  when  $z = 0$  ( $j = 0, 1, 2, \dots, 90$ ). Let  $s_{n,j}$  be the number of non escaping initial conditions after  $n$  years (we are using the same mesh as before), around the orbit  $C_j$ . Let  $s_n$  be  $\sum_j s_{n,j}$ , that is,  $s_n$  denotes the total number of non escaping points around VF3. The values of  $s_n$ , for  $n$  ranging between 100 and 1 000 years are displayed in Fig. 13. We have tried several fits to these data, trying to show the persistence of a certain number of points when  $n$  goes to infinity (Simó et al. 1995), but the results are inconclusive. It turns out that the number of remaining points strongly depends on the fitting function used, and there are no theoretical reasons for suggesting any particular type of fitting function. We think that longer numerical integrations will help to elucidate this question.

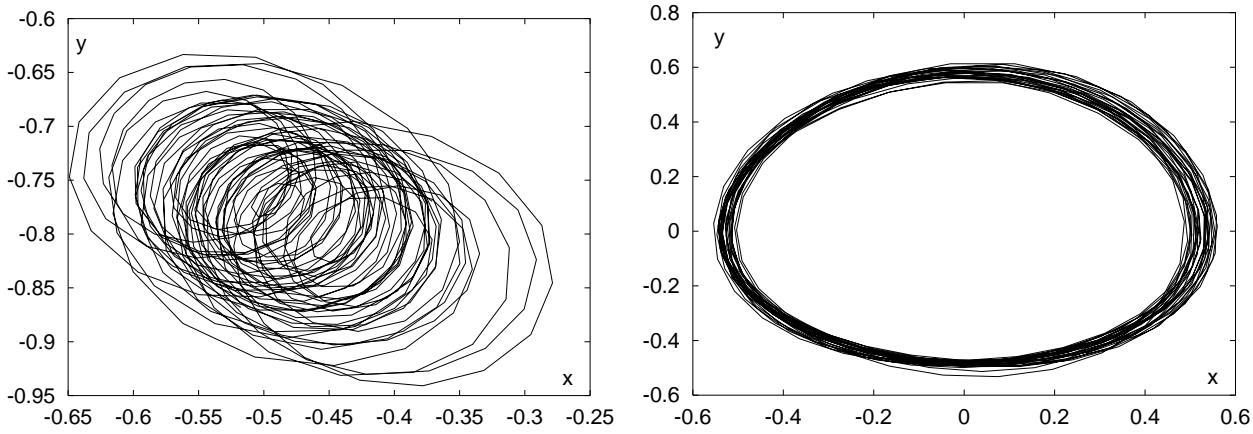


**Fig. 14.** Trajectory inside the stability region of the JPL model, corresponding to the slice  $\dot{z} = 0.58$  ( $L_4$  case). Left plot:  $(x, y)$  projection; right plot:  $(z, \dot{z})$  projection. Integration time: 2 years.

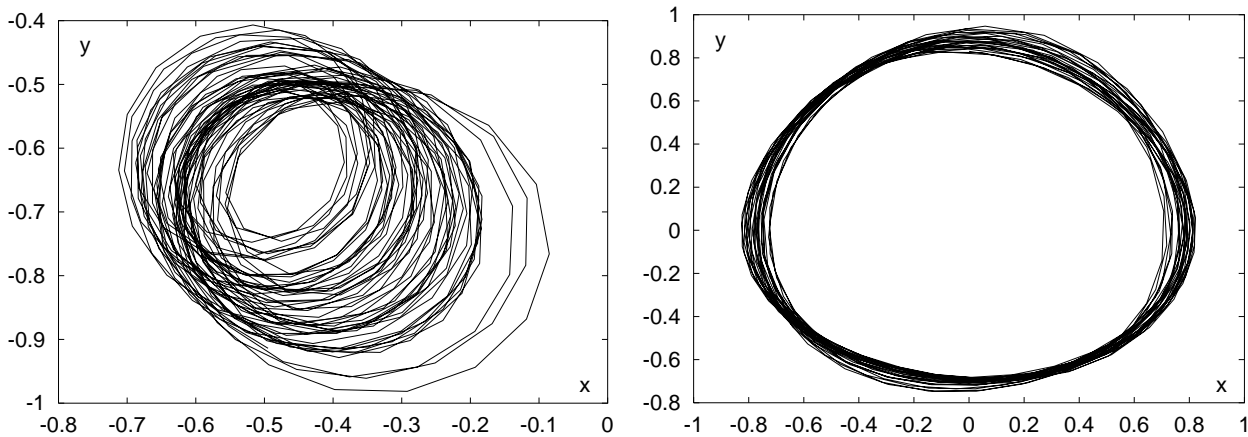


**Fig. 15.** Trajectory inside the stability region of the JPL model, corresponding to the slice  $\dot{z} = 0.83$  ( $L_4$  case). Left plot:  $(x, y)$  projection; right plot:  $(z, \dot{z})$  projection. Integration time: 2 years.

### 3.2. Typical trajectories in the stable region

To explain the dynamics inside the quasi-stable region, we first show a few trajectories corresponding to the slices  $\dot{z} = 0.58$  and  $\dot{z} = 0.83$  (see Fig. 10). In each slice, we have selected an initial condition near the “central part” of the stable region. For each initial condition, we have computed the corresponding orbit in the JPL model, for the  $L_4$  case, and the results are displayed in Figs. 14 and 15 (similar figures are obtained for the  $L_5$  case). To give a sense of velocity we have drawn the orbit as a polygonal line, putting a vertex for each day of the integration.

It is interesting to look at the  $(z, \dot{z})$  projection of these trajectories. They show that the vertical oscillations are very close to an harmonic oscillator: there is a clear frequency that dominates this motion and the remaining frequencies appear as a perturbation. This dominating frequency is already contained in the BCP and RTBP (it is related to the vertical frequency of the  $L_{4,5}$  points in the RTBP and to the vertical frequency of the orbits PO1, PO2 and PO3 of the BCP), and its period is a little less than a month.

## 4. Technical details

The numerical integrations for the BCP model have been performed using a Taylor method of order 20 (Jorba & Zou 2000). The numerical integrations for the JPL model have been carried out by a standard Runge-Kutta-Fehlberg method of orders 7 and 8. A sample of the results has been tested –on a different computer– against a third numerical integrator, the Shampine-Gordon method (Shampine & Gordon 1975). The results obtained are quite similar, with very small differences that seem to come from the different arithmetic and truncation errors.

The numerical integrations for the JPL model have been performed as follows. From the data in the JPL ephemeris file, we compute the equatorial coordinates of each planet (with origin at the instantaneous centre of mass of the Solar system), except for the Moon whose coordinates are referred to the Earth. From a numerical point of view, it is not a good idea to have the origin of coordinates at the centre of mass of the Solar system because then the different coordinates of the trajectories near the triangular points of the Earth-Moon system are very close, and this could result in cancellations of meaningful digits. For this

reason, the origin of the coordinates has been translated to the Earth-Moon barycentre. The ideas for these tasks are described in Gómez et al. (1985; 1987; 1991; 1993).

## 5. Conclusions

One of the main issues of this work is to show the existence of regions of practical stability near the equilateral points of the real Earth-Moon system. As the classical RTBP model is not close enough to the real system, we have used a suitable intermediate model, the BCP. The study of this model has revealed the existence of quasi-stable regions, but outside the Earth-Moon plane. Finally, these regions have been numerically checked against a realistic model of the Solar system obtained from the JPL ephemeris. In this way, we avoid carrying out massive numerical simulations on the JPL model that could result in a prohibitive need of computer time. The results show that a relevant part of the stable regions of the BCP persists in the JPL, at least for 1 000 years.

A natural question is the persistence of these regions for longer time intervals. From the results presented here, we cannot give a conclusive answer to this question. We are currently working on this problem by using improved versions of the BCP, taking into account the Moon's eccentricity and inclination. The regions obtained for these models will be tested against longer numerical integrations of the Solar system. We believe that better models can give a deeper insight into many features of the dynamics, like the role played by resonances in the size and shape of these regions. Moreover, a more accurate determination of these regions could help to extend the quasi-stability times.

One of the possible reasons for interest in the regions around the family VF3 is that they could be a suitable place to look for some kind of dust or even some small asteroids. In this case, it would not be very difficult to send a probe there to pick up some samples. Moreover, these regions plus the regions around the family VF2 could also be of interest for some space missions, since no control is necessary to keep a spacecraft there.

The typical motion for a particle inside this region has been shown in Figs. 14 and 15. As has been mentioned in Sect. 3.2, it is clear that the largest part of the region corresponds to trajectories that cut the Earth-Moon plane with vertical speeds (relative to that plane) close to either 0.58 or 0.83, in adimensional units. This corresponds to speeds close to either 0.56 or 0.80 km s<sup>-1</sup>. We note that the motion in the vertical direction is very close to an harmonic oscillator (with a period of a little less than a month), and that these trajectories reach an approximate angular separation over (or under) the Earth-Moon plane of either 30 or 40 degrees. Hence, as it happens in a typical harmonic oscillator, the trajectories must spend most of the time away from the Earth-Moon plane and near their maximum elongation. Then, to have the best chance of finding Trojan asteroids in the Earth-Moon system, one should focus the search around either 30 or 40 degrees over (and under) the Earth-Moon plane. Performing the search near that plane has a much lower chance of success and, even in this case, it can be difficult to con-

firm an observation since the asteroid is moving at its highest speed. In fact, there are records of a few observations of small dust clouds near the Earth-Moon Lagrangian points, but none of them has been confirmed subsequently (Freitas & Valdes 1980; Valdes & Freitas 1983).

*Acknowledgements.* I am indebted with J. Masdemont for his version of the code developed in Gómez et al. (1985; 1987; 1991; 1993) to work with the JPL ephemeris. I also want to acknowledge interesting discussions with C. Simó, and the comments of S. Haberman on a preliminary version of the paper. This research has been supported by the Spanish grant DGICYT PB94-0215 and the Catalan grant CIRIT 1998S0GR-00042. The numerical simulations have been carried out on Hidra, the Beowulf cluster of the UB-UPC Dynamical Systems Group (<http://www.maia.ub.es/dsg/hidra>).

## References

- Arnold V., 1964, *Soviet Math. Dokl.* 5, 581  
 Arnold V., Kozlov V., Neishtadt A., 1988, *Dynamical Systems III*, Vol. 3 of *Encyclopaedia Math. Sci.*, Springer, Berlin  
 Benettin G., Fassò F., Guzzo M., 1998, *Regul. Chaotic Dyn.* 3(3), 56  
 Castellà E., Jorba À., 2000, *Cel. Mech.* 76(1), 35  
 Celletti A., Giorgilli A., 1991, *Cel. Mech.* 50(1), 31  
 Companys V., Gómez G., Jorba À., et al., 1996, In: Alfriend K., Ross I., Misra A., Peters C. (eds.) *AAS/AIAA Astrodynamics Conference, Advances in the Astronautical Sciences*. Vol. 90, AAS, San Diego, USA, p. 1655  
 Cronin J., Richards P., Russell L., 1964, *Icarus* 3, 423  
 Díez C., Jorba À., Simó C., 1991, *Cel. Mech.* 50(1), 13  
 Freitas R., Valdes F., 1980, *Icarus* 42, 442  
 Giorgilli A., Delshams A., Fontich E., Galgani L., Simó C., 1989, *J. Diff. Eq.* 77, 167  
 Giorgilli A., Skokos C., 1997, *A&A* 317, 254  
 Gómez G., Jorba À., Masdemont J., Simó C., 1991, Study refinement of semi-analytical Halo orbit theory. ESOC contract 8625/89/D/MD(SC), final report, European Space Agency  
 Gómez G., Jorba À., Masdemont J., Simó C., 1993, Study of Poincaré Maps for Orbits near Lagrangian Points. ESOC contract 9711/91/D/IM(SC), final report, European Space Agency  
 Gómez G., Llibre J., Martínez R., Simó C., 1985, Station keeping of libration point orbits. ESOC contract 5648/83/D/JS(SC), final report, European Space Agency  
 Gómez G., Llibre J., Martínez R., Simó C., 1987, Study on orbits near the triangular libration points in the perturbed Restricted Three-Body Problem. ESOC contract 6139/84/D/JS(SC), final report, European Space Agency  
 Jorba À., 1998, *Proceedings of the III International Symposium HAMSYS-98. Geometrical Methods in Hamiltonian Systems and Celestial Mechanics*. Pátzcuaro (México), December 7-11, 1998, World Scientific (to appear).  
 Jorba À., 2000, Numerical computation of the normal behaviour of invariant curves of  $n$ -dimensional maps, preprint, 2000  
 Jorba À., Simó C., 1994, In: Seimenis J. (ed.), *Hamiltonian Mechanics: Integrability and Chaotic Behaviour*. NATO Adv. Sci. Inst. Ser. B Phys. Vol. 331, Toruń, Poland, 28 June-2 July 1993, Plenum, New York, p. 245  
 Jorba À., Villanueva J., 1997a, *Nonlinearity* 10, 783  
 Jorba À., Villanueva J., 1997b, *J. Nonlinear Sci.* 7, 427  
 Jorba À., Villanueva J., 1998, *Phys. D* 114, 197

- Jorba À., Zou M., 2000, On the numerical integration of ODE by means of high-order Taylor methods. in preparation.
- McKenzie R., Szebehely V., 1981, *Cel. Mech.* 23(3), 223
- Meyer K.R., Hall G.R., 1992, *Introduction to Hamiltonian Dynamical Systems and the N-Body Problem*. Springer, New York
- Niederman L., 1998, *Nonlinearity* 11(5), 1465
- Schutz B., Tapley B., 1970, In: Giacaglia G. (ed.) *Periodic Orbits, Stability and Resonances*. D. Reidel Publishing Company, Dordrecht, Holland, p. 128
- Shampine L.F., Gordon M.K., 1975, *Computer solution of Ordinary Differential Equations*. Freeman, San Francisco
- Simó C., 1989, *Mem. Real Acad. Cienc. Artes Barcelona* 48(7), 303
- Simó C., Jorba À., Masdemont J., Gómez G., 1995, In: Roy A., Steves B. (eds.) *From Newton to Chaos*. Plenum Press, New York, p. 343
- Szebehely V., 1967, *Theory of Orbits*. Academic Press
- Szebehely V., Premkumar R., 1982, *Cel. Mech.* 28, 195
- Valdes F., Freitas R., 1983, *Icarus* 53, 453